Front. Mater. Sci. 2016, 10(1): 45–55
DOI 10.1007/s11706-016-0326-z

RESEARCH ARTICLE

Heterogeneous Fenton-like discoloration of methyl orange using Fe_3O_4/MWCNTs as catalyst: process optimization by response surface methodology

Huan-Yan XU (✉), Tian-Nuo SHI, Hang ZHAO, Li-Guo JIN, Feng-Chun WANG, Chun-Yan WANG, and Shu-Yan QI

School of Materials Science and Engineering, Harbin University of Science and Technology, Harbin 150040, China

ABSTRACT: **Fe_3O_4/MWCNTs nanocomposites were prepared by chemical oxidation coprecipitation method and developed as highly efficient heterogeneous Fenton-like catalyst. XRD results revealed that Fe_3O_4 nanoparticles deposited onto MWCNTs surface remained the inverse spinel crystal structure of cubic Fe_3O_4 phase. The FTIR characteristic peaks of MWCNTs weakened or disappeared due to the anchor of Fe_3O_4 nanoparticles and Fe–O peak at 570 cm^{-1} was indicative of the formation of Fe_3O_4. TEM observation revealed that Fe_3O_4 nanoparticles were tightly anchored by MWCNTs. The Fenton-like catalytic activity of Fe_3O_4/MWCNTs nanocomposites for the discoloration of methyl orange (MO) was much higher than that of Fe_3O_4 nanoparticles. The process optimization of this heterogeneous Fenton-like system was implemented by response surface methodology (RSM). The optimum conditions for MO discoloration were determined to be of 12.3 mmol/L H_2O_2 concentration, 2.9 g/L catalyst dosage, solution pH 2.7 and 39.3 min reaction time, with the maximum predicted value for MO discoloration ratio of 101.85%. The corresponding experimental value under the identical conditions was obtained as 99.86%, which was very close to the predicted one with the absolute deviation of 1.99%.**

KEYWORDS: **Fe_3O_4/MWCNTs; Fenton-like catalyst; azo dye; response surface methodology**

Contents

Received October 13, 2015; accepted November 20, 2015

E-mail: xhy7587@aliyun.com

1 Introduction

Textile dyes constitute one of the largest groups of organic contaminants that represent an increasing environmental danger. Discoloration of dye effluents has therefore received increasing attention [1]. Due to slow biodegradability and harmful intermediates, azo dyes are one of the major concerns for waste management [2]. Various technologies have been developed for effective degradation or discoloration of contaminated water by azo dyes. Dye removal from waste water can be categorized based on adsorption and degradation. Presently, the technology of advanced oxidation processes (AOPs) based on Fenton's chemistry is successful for degradation of various types of dyes [3]. Due to the limitations of homogeneous Fenton reaction, such as narrow working pH range (pH < 3), separation and recovery of metal ion and formation of iron oxide sludge, various heterogeneous Fenton-like catalysts have recently been developed and used over a wider pH range for the degradation of organic pollutants [4]. In this case, low-cost minerals or inorganic materials with special crystal structures or properties are the best alternatives as heterogeneous Fenton catalysts, behaving as the iron supporter or container.

Among heterogeneous Fenton-like catalysts, iron minerals, such as goethite (α-FeOOH), magnetite (Fe_3O_4) and pyrite (FeS_2), have been extensively investigated because of their relatively wide availability in the soil environment and simple operation conditions [5]. Therein, Fe_3O_4 is regarded as one of the most promising Fenton-like catalysts, attributed to the simultaneous presence of Fe (II) and Fe(III) in the octahedral structure. This characteristic can allow Fe species to be reversibly oxidized and reduced without structural change. According to the Haber–Weiss mechanism, the coexistence of Fe(II) and Fe(III) helps to increase the catalytic decomposition of hydrogen peroxide (H_2O_2) to generate highly oxidative hydroxyl radical (·OH) and enhance the degradation of organic contaminants [6]. Furthermore, as an inverse spinel crystal, Fe_3O_4 exhibits good magnetic properties and can be completely separated from the liquid medium by an external magnet [7–8]. Although decreasing the particle size can improve Fenton-like catalytic activity of Fe_3O_4 [9], Fe_3O_4 nanoparticles are easy to aggregate in water. To address this problem, the dispersed immobilization of Fe_3O_4 nanoparticles has been pursued on various materials such as bentonite [10], alginate beads [11], chitosan hollow fibers [12], carbon nanotubes [13–17], porous carbonaceous matrix [18], activated carbon [19], graphene oxide [20–22] and so on. Carbon nanotubes (CNTs), categorized as single-walled carbon nanotubes (SWCNTs) and multi-walled carbon nanotubes (MWCNTs), can be regarded as rolled graphene sheets held together by van der Waals bonds. CNTs have great potential applications in various fields such as biosensor, nanobiotechnology and others, due to the electrical conductivity and stability toward chemical reaction [23]. Due to large surface area and good surface properties, MWCNTs have been widely employed as the carrier of Fe_3O_4 nanoparticles to enhance the catalytic activity of heterogeneous Fenton-like reaction for the degradation of different organic pollutants. Yu et al. found that Fe_3O_4/MWCNTs showed a higher utilization efficiency of H_2O_2, higher adsorption ability for atrazine (ATZ) and higher degradation efficiency of ATZ than Fe_3O_4 nanoparticles in heterogeneous Fenton-like reaction. The effects of solution pH, catalysts dosage, H_2O_2 concentration and iron leaching on the degradation of ATZ were investigated [17]. Zhou et al. reported that Fe_3O_4/MWCNTs were used as a heterogeneous Fenton-like catalyst for the degradation of tetrabromobisphenol A (TBBPA). A degradation pathway for this system was proposed following analysis of intermediate products. The quantification of Fe^{2+} and Fe^{3+} distribution before and after the recycling test of the composite were explored [16]. Cleveland et al. employed Fe_3O_4/MWCNTs as heterogenous Fenton-like catalyst for the effective degradation of aqueous bisphenol A (BPA). The scavenging tests of the hydroxyl radicals suggested that the ·OH-driven oxidation was the major step among the multiple reactions in the heterogeneous Fenton-like oxidation [13]. Moreover, Fe_3O_4/MWCNTs were used as a Fenton-like catalyst to decompose Acid Orange II and displayed a higher activity than nanometer-size Fe_3O_4. The superparamagnetism of Fe_3O_4/MWCNTs at room temperature was investigated [14]. A trace steroidal endocrine disrupting compound (EDC) 17α-methyltestosterone (MT) in water could be removal by Fe_3O_4/MWCNTs in presence of H_2O_2. The synergy mechanism of adsorption and degradation was proposed [15]. However, to our best knowledge, the process optimization about Fe_3O_4/MWCNTs–H_2O_2 Fenton-like system has not been involved up to now, which would be beneficial to the engineering aspects.

Hence, in the present study, based on the fabrication and characterization of Fe_3O_4/MWCNTs nanocomposite, we focused on the process optimization of the heterogeneous Fenton-like discoloration of an azo dye, methyl orange

(MO) by Fe_3O_4/MWCNTs in presence of H_2O_2, using the response surface methodology (RSM).

2 Materials and methods

2.1 Preparation of Fe_3O_4/MWCNTs

The anchor of Fe_3O_4 nanoparticles onto MWCNTs was realized by chemical oxidation coprecipitation method. Due to the tendency to agglomerate in any solvent, pristine MWCNTs are difficult to disperse uniformly. To solve this problem, functionalization of MWCNTs with nitric acid has been widely reported [24]. In a typical procedure of the pretreatment of MWCNTs, 500 mg of MWCNTs were put into a flask that contained 320 mL mixed solution of sulfuric acid (H_2SO_4) and nitric acid (HNO_3) with a volume ratio of 3:1, and then the mixture undertook a ultrasonic processing with refluxing for 3 h. After filtrated, repeatedly washed with deionized water and dried at 80°C in a vacuum oven for 8 h, the functionalized MWCNTs were obtained for further use. The anchor of Fe_3O_4 nanoparticles onto MWCNTs was implemented as the following procedures. 0.5 g functionalized MWCNTs were added into 400 mL deionized water and treated by ultrasonication for 20 min. Then, 7.4 g $FeSO_4\cdot 7H_2O$ was added while keeping ultrasound on. After $FeSO_4\cdot 7H_2O$ was dissolved completely, the suspension solution was transferred to a water-bath pot and heated to 95°C with vigorous mechanical stirring. Subsequently, 160 mL solution with 6.66 g NaOH and 3.33 g $NaNO_3$ was added dropwise and then the as-obtained solution was kept at 95°C for 2 h with vigorous stirring during the whole period. After cooled to room temperature, the precipitate was separated by a magnet and washed 3 times with deionized water and anhydrous alcohol, respectively, under ultrasound for 5 min. After dried at 60°C in a vacuum oven overnight, Fe_3O_4/MWCNTs nanocomposites with estimated 80 wt.% Fe_3O_4 content was obtained. As comparison, pure Fe_3O_4 nanoparticles were also prepared using the same procedure except for the addition of functionalized MWCNTs.

2.2 Characterization techniques

X-ray diffraction (XRD) was employed to determine the crystalline phases of functionalized MWCNTs, Fe_3O_4 nanoparticles and Fe_3O_4/MWCNTs nanocomposites and recorded on a Rigaku D/max-3B X-ray diffractometer over the 2θ range of 20°–80° with the scanning rate of 8(°)/min. Fourier transform infrared spectroscopy (FTIR) was used to confirm the chemical groups in the obtained samples and measured on a Nicolet Nexus infrared spectrometer after sample was mixed with 300 mg of spectroscopic grade KBr and pressed into thin slices. The microstructure of the obtained samples was observed by transmission electron microscopy (TEM, JEOL JEM-2010, Japan) at an accelerating voltage of 200 kV.

2.3 Heterogeneous Fenton-like experiments

An azo dye, MO was employed as the target pollutant for this study. A stock solution containing MO (100 mg/L) was prepared and subsequently diluted to the required concentration for the Fenton-like tests. The solution pH was adjusted by the addition of NaOH and HNO_3. Then, a certain gram of the catalyst was added into 100 mL of the solution with required MO concentration. After the addition of hydrogen peroxide (H_2O_2, 30% (w/w)), the heterogeneous Fenton-like test was implemented under magnetic stirring. At regular time intervals of reaction, 2 mL of the reaction solution was collected for the measurement of MO concentration using a 752-type ultraviolet (UV)-vis spectrophotometer at a wavelength of 482 nm. The discoloration ratio of MO was calculated by the following equation: $D_R/\% = [(C_0 - C_t)/C_0]\times 100$, where C_0 is the initial MO concentration and C_t the residual MO concentration at the reaction time t. In order to check the reproducibility of the results, random tests were done for different experimental conditions.

2.4 Experimental design, analysis and optimization

The central composite design (CCD) under RSM was employed for the experimental design and process optimization of MO discoloration process in Fe_3O_4/MWCNTs–H_2O_2 Fenton-like system.

Four factors, in this work, were selected as independent variables, i.e. solution pH (X_1), H_2O_2 concentration (X_2, mmol/L), catalyst dosage (X_3, g/L), and reaction time (X_4, min). The percentage of the discoloration ratio of MO was chosen as the output variable (response). According to the typical temperature of real dyeing wastewater [25], MO simulated wastewater was maintained at 50°C for all designed experiments. The experimental design, mathematical modeling and optimization were performed with the Design Expert 8.0.7.1 software (Stat-Ease, Inc.). For statistical calculations, the variables X_i were coded as x_i

according to the following equation [26]:

$$x_i = \frac{X_i - X_0}{\delta X} \quad (1)$$

where x_i is the code value, X_i is the uncoded value, X_0 is the value of X_i at the center point, and δX presents the step change. The experimental ranges and levels of the independent variables for MO discoloration are illustrated in Table 1, which were determined by our preliminary studies. A second-order regression model was employed to analyze and fit the responses to the independent variables, shown in Eq. (2) [27–28]:

$$Y = \beta_0 + \sum_{i=1}^{k} \beta_i X_i + \sum_{i=1}^{k} \beta_{ii} X_i^2 + \sum_i \sum_j \beta_{ij} X_i X_j \quad (2)$$

where Y is response (MO discoloration ratio); X_i and X_j input variables that influence the response (Y); β_0 an intercept constant; β_i the first-order regression coefficient; β_{ii} the second-order regression coefficient representing quadratic effect of factor i; and β_{ij} the coefficient of interaction between factors i and j.

3 Results and discussion

3.1 Characterization of Fe_3O_4/MWCNTs

Figure 1 illustrates XRD patterns of the acid-treated MWCNTs, Fe_3O_4 nanoparticles and Fe_3O_4/MWCNTs nanocomposites. For the acid-treated MWCNTs, the characteristic graphitic peaks centred at 25.8° and 42.9° [29–30] are ascribed to the (002) and (100) crystal planes, respectively, referring to the standard XRD data JCPDS 26-1080. This result indicates that the MWCNTs structure was not destroyed after treatment by mixed acids [31]. For Fe_3O_4 nanoparticles, seven distinctive peaks can be found at 2θ of 18.3°, 30.1°, 35.5°, 43.2°, 53.7°, 57.2° and 62.6°, matching well with the crystal planes of (111), (220), (311), (400), (422), (511) and (440) for the cubic Fe_3O_4 phase of inverse spinel crystal structure (JCPDS 65-3107), respectively. After deposition of Fe_3O_4 nanoparticles onto the surface of MWCNTs, the seven XRD peaks of Fe_3O_4 phase remain unchanged and no other peaks corresponding to impurities can be detected, suggesting that the Fe_3O_4 nanoparticles in the nanocomposites are pure Fe_3O_4 with the inverse spinel structure.

FTIR spectra of the acid-treated MWCNTs and Fe_3O_4/MWCNTs nanocomposites are shown in Fig. 2. The FTIR absorption peaks at 1650 and 1397 cm^{-1} in the spectrum of acid-treated MWCNTs are the characteristic bands of graphite structure and disordered structure of MWCNTs, respectively [32], also indicating the unchanged structure of MWCNTs after the acid treatment. The peak at 3361 cm^{-1} can be assigned to –OH stretching vibration mode in carboxyl groups or adsorbed water. The shift in characteristic wavenumber to the lower direction indicates the presence of strong hydrogen bonds between –OH groups [33–34]. The peaks at 2976 and 2899 cm^{-1} can be related to the asymmetric and symmetric –CH stretching vibration mode of the sidewalls [35]. The absorption peak at 1703 cm^{-1} for the acid-treated MWCNTs clearly indicates the formation of carboxyl functional groups (–COOH) [33]. The bands in the range of 1300–950 cm^{-1} prove the presence of C–O bonds in various chemical surroundings [34]. The formation of these functional groups during acid treatment would facilitate the anchor of Fe_3O_4 nanoparticles on the surface of acid-treated MWCNTs via a hydrogen bond and van der Waals forces. Nevertheless, the absorption peaks of these functional groups weaken or disappear in the spectrum of Fe_3O_4/MWCNTs nanocomposites, suggesting that these groups were depleted during the chemical oxidation coprecipitation of Fe_3O_4 nanoparticles. Meanwhile, the Fe–O characteristic peak can be observed near the wavenumber of 570 cm^{-1}, which is indicative of the formation of Fe_3O_4 [36].

TEM images of the acid-treated MWCNTs and Fe_3O_4/MWCNTs nanocomposites are shown in Fig. 3. Figure 3(a) reveals that, although there are some knobs in the treated MWCNTs and a distortion in the linearity of its structure, the MWCNTs still maintains tubular crystal structure [31].

Table 1 Variables and their codes and real experimental values used in CCD

Coded level	Variables			
	Solution pH, X_1	H_2O_2 concentration, X_2 /(mmol·L^{-1})	Catalyst dosage, X_3 /(g·L^{-1})	Reaction time, X_4 /min
−2	1	9.69	1.0	10
−1	2	19.35	2.0	20
0	3	29.07	3.0	30
1	4	38.76	4.0	40
2	5	48.45	5.0	50

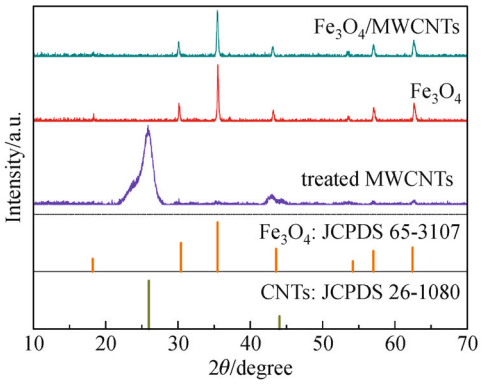

Fig. 1 XRD patterns of acid-treated MWCNTs, Fe_3O_4 nanoparticles and Fe_3O_4/MWCNTs nanocomposites.

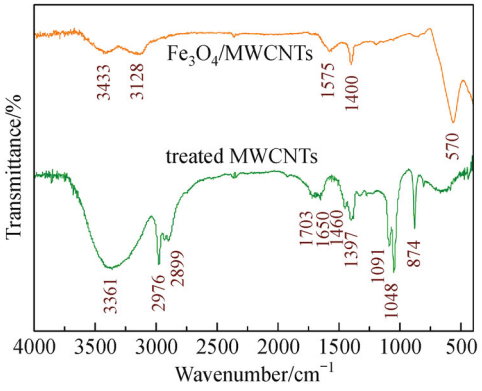

Fig. 2 FTIR spectra of acid-treated MWCNTs and Fe_3O_4/MWCNTs nanocomposites.

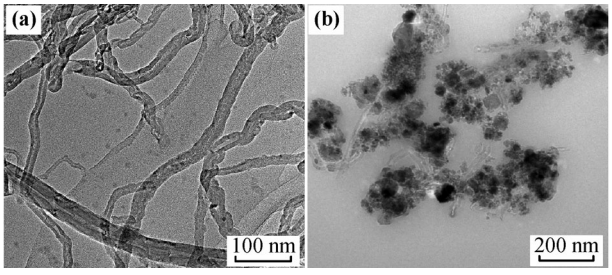

Fig. 3 TEM images of **(a)** acid-treated MWCNTs and **(b)** Fe_3O_4/MWCNTs nanocomposites.

Furthermore, good dispersion of the acid-treated MWCNTs can be seen, indicating that the surface modification of MWCNTs with H_2SO_4/HNO_3 can efficiently improve the dispersion of MWCNTs. Figure 3(b) illustrates that Fe_3O_4 nanoparticles are tightly anchored by the acid-treated MWCNTs. Even after repeated dispersion in water under ultrasonication for the preparation of TEM sample, almost all Fe_3O_4 nanoparticles were still grasped by MWCNTs, which suggested that the Fe_3O_4 nanoparticles were not simply absorbed on the surface of MWCNTs, but combined with MWCNTs via a strong interaction [31].

3.2 Heterogeneous Fenton-like trials

In this study, contrast experiments were operated to evaluate the heterogeneous Fenton-like efficiency of Fe_3O_4/MWCNTs nanocomposites. The discoloration of MO was investigated in Fe_3O_4–H_2O_2, MWCNTs–H_2O_2, Fe_3O_4/MWCNTs–H_2O_2, Fe_3O_4, MWCNTs and Fe_3O_4/MWCNTs systems, respectively, and the results are shown in Fig. 4. In Fe_3O_4–H_2O_2 system, Fe_3O_4 nanoparticles were employed as the heterogeneous Fenton-like catalyst. It can be observed from Fig. 4 that MO discoloration ratio increases with the reaction time prolonging and reaches only 57% at 60 min. This result indicates that Fe_3O_4 nanoparticles exhibit a poor catalysis for H_2O_2-driven discoloration of MO, consistent with the report by Deng et al. [14]. In Fe_3O_4 system, Fe_3O_4 nanoparticles only acted as adsorbents for MO discoloration, with lower adsorption capacity for MO molecules. In MWCNTs and MWCNTs–H_2O_2 systems, MO discoloration behaviour is parallel as illustrated in Fig. 4. Compared with Fe_3O_4 nanoparticles, MWCNTs displayed more adsorption capacity for MO molecules, attributed to the larger surface area. Furthermore, due to the absence of iron ions in MWCNTs, H_2O_2 could not be triggered in MWCNTs–H_2O_2 system. However, when Fe_3O_4/MWCNTs nanocomposites were used as the heterogeneous Fenton-like catalyst under the identical conditions, MO discoloration ratio could approach 100%, suggesting that Fe_3O_4/MWCNTs nanocomposites had much better Fenton-like catalytic activity than Fe_3O_4 nanoparticles. In Fe_3O_4/MWCNTs system, due to the absence of H_2O_2, Fe_3O_4/MWCNTs nanocomposites actually acted as the adsorbents. It can be seen from Fig. 4 that, in this system, the equilibrium between adsorption and desorption is established within 40 min reaction time with MO discoloration ratio near 41%. The discoloration ratio of MO in Fe_3O_4/MWCNTs–H_2O_2 system is 2.5 times more than that in Fe_3O_4/MWCNTs system, implying that it is the heterogeneous Fenton-like reaction that governs the discoloration process of MO. It cannot be denied that the positive effect of adsorption would enhance the catalytic activity of Fe_3O_4/MWCNTs in heterogeneous Fenton-like system [31].

3.3 Experimental design by CCD under RSM

The design consisted of 2^k factorial points augmented by $2k$

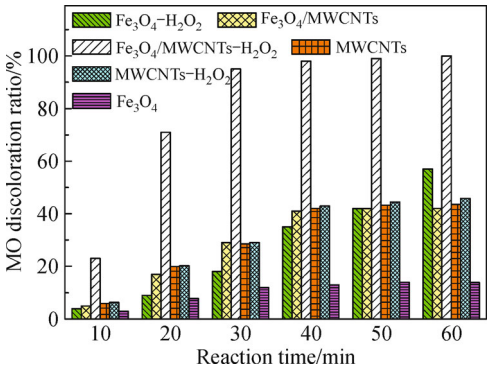

Fig. 4 Contrast experiments of 50 mg/L MO discoloration at room temperature in Fe_3O_4–H_2O_2 system (pH = 2, $[H_2O_2]_0$ = 19.38 mmol/L, Fe_3O_4 dosage = 2.0 g/L), Fe_3O_4/MWCNTs system (pH = 2, Fe_3O_4/MWCNTs dosage = 2.0 g/L), Fe_3O_4/MWCNTs–H_2O_2 system (pH = 2, $[H_2O_2]_0$ = 19.38 mmol/L, Fe_3O_4/MWCNTs dosage = 2.0 g/L), MWCNTs system (pH = 2, MWCNTs dosage = 2.0 g/L), MWCNTs–H_2O_2 system (pH = 2, $[H_2O_2]_0$ = 19.38 mmol/L, MWCNTs dosage = 2.0 g/L) and Fe_3O_4 system (pH = 2, Fe_3O_4 dosage = 2.0 g/L).

axial points and a center point, where k is the number of variables (4 in this case). Accordingly, 30 experiments, with 4 factors and 5 levels for each factor were designed, as listed in Table 2. Among these 30 experiments, 6 experiments were repetition of the central point (run Nos. 3, 14, 18, 19, 24 and 26). The closeness of the responses of these 6 experiments can be a sign of the accuracy of the experiment process [37]. The results obtained from the present experimental design are also presented in Table 2.

3.4 Regression models and statistical testing

For predicting the optimal values of MO discoloration within the experimental conditions, a second order polynomial model was fitted to the experimental results for MO discoloration ratio. The obtained polynomial model is shown as the following equation:

Table 2 Central composite design matrix along with the experimental and predicted values of MO discoloration ratio

Run	X_1	X_2	X_3	X_4	MO discoloration ratio, Y /%	
					Experimental	Predicted
1	0	2	0	0	63.35	64.91
2	0	0	0	−2	15.09	15.32
3	0	0	0	0	89.73	89.20
4	1	−1	−1	−1	38.10	35.95
5	1	1	1	1	86.77	84.16
6	−1	1	−1	1	74.57	70.23
7	1	−1	1	1	97.48	98.32
8	0	−2	0	0	92.77	90.55
9	2	0	0	0	79.98	78.99
10	−1	−1	−1	1	85.68	84.59
11	−1	1	1	−1	85.43	82.48
12	1	1	−1	−1	11.67	8.94
13	−1	1	1	1	98.42	102.61
14	0	0	0	0	90.42	89.20
15	1	−1	1	−1	69.88	72.84
16	−1	−1	1	1	98.98	100.78
17	1	1	−1	1	63.99	66.07
18	0	0	0	0	88.76	89.20
19	0	0	0	0	89.18	89.20
20	−1	1	−1	−1	13.92	15.11
21	0	0	2	0	92.08	88.76
22	−1	−1	−1	−1	25.34	26.58
23	0	0	0	2	96.79	95.91
24	0	0	0	0	90.42	89.20
25	−1	−1	1	−1	77.82	77.77
26	0	0	0	0	86.70	89.20
27	0	0	-2	0	16.83	19.49
28	−2	0	0	0	87.73	88.06
29	1	1	1	−1	58.44	61.57
30	1	−1	−1	1	94.85	96.42

$$Y = 89.20 - 2.27X_1 - 6.41X_2 + 17.32X_3 + 20.15X_4 - 1.42X_1^2 - 2.87X_2^2 - 8.77X_3^2 - 8.40X_4^2 - 4.00X_1X_2 - 3.57X_1X_3 + 0.62X_1X_4 + 4.05X_2X_3 - 0.72X_2X_4 - 8.75X_3X_4 \quad (3)$$

Statistical testing of this model was implemented by analysis of variance (ANOVA) and the results are shown in Table 3, which indicate that the derived quadratic polynomial model is significant. Figure 5 suggests that the predicted discoloration ratios of MO agree well with the experimental values, also indicating a high significance of the model. Through constructing the plot of studentized residuals *vs.* the normal of probability (Fig. 6), a check was made for the normality assumption, which was found to be satisfied for MO discoloration.

3.5 Three-dimensional (3D) response surface analysis

The 3D response surface diagrams for the interaction between two variables are presented in Figs. 7–12 with different interactions of (i) solution pH (X_1) and H_2O_2 concentration (X_2), (ii) solution pH (X_1) and catalyst dosage (X_3), (iii) solution pH (X_1) and reaction time (X_4), (iv) H_2O_2 concentration (X_2) and catalyst dosage (X_3), (v) H_2O_2 concentration (X_2) and reaction time (X_4), and (vi) catalyst dosage (X_3) and reaction time (X_4), respectively. From these response surface diagrams, it can be observed that the interactions between two independent variables are not significant, because the curvature of 3D surfaces is

Table 3 ANOVA for the obtained quadratic polynomial model

Source	Sum of squares	Degree of freedom	Mean square	F value	p-value (Prob > F)	
Model	23580.71	14	1684.34	184.14	< 0.0001	Significant
X_1	123.67	1	123.67	13.52	0.0022	
X_2	985.09	1	985.09	107.69	< 0.0001	
X_3	7196.81	1	7196.81	786.79	< 0.0001	
X_4	9742.12	1	9742.12	1065.05	< 0.0001	
X_1X_2	255.68	1	255.68	27.95	< 0.0001	
X_1X_3	204.35	1	204.35	22.34	0.0003	
X_1X_4	6.08	1	6.08	0.66	0.4278	
X_2X_3	261.79	1	261.79	28.62	< 0.0001	
X_2X_4	8.35	1	8.35	0.91	0.3544	
X_3X_4	1224.65	1	1224.65	133.88	< 0.0001	
X_1^2	55.23	1	55.23	6.04	0.0267	
X_2^2	225.57	1	225.57	24.66	0.0002	
X_3^2	2109.11	1	2109.11	230.58	< 0.0001	
X_4^2	1934.30	1	1934.30	211.47	< 0.0001	
Residual	137.21	15	9.15			
R^2	0.9942					
Adj R^2	0.9888					

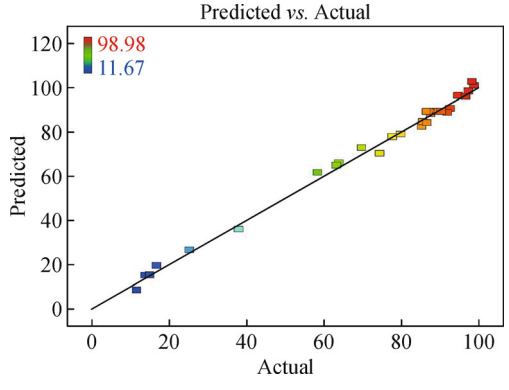

Fig. 5 Predicted *vs.* actual values plot for MO discoloration.

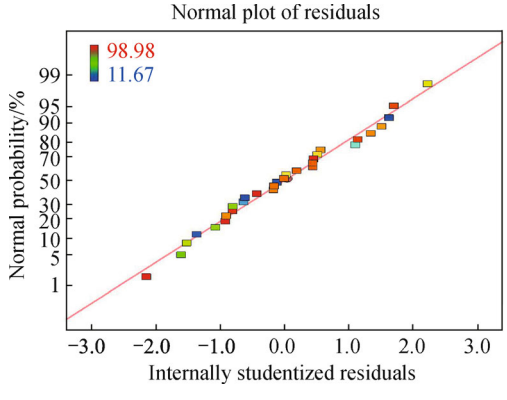

Fig. 6 Normal plot of residuals for MO discoloration.

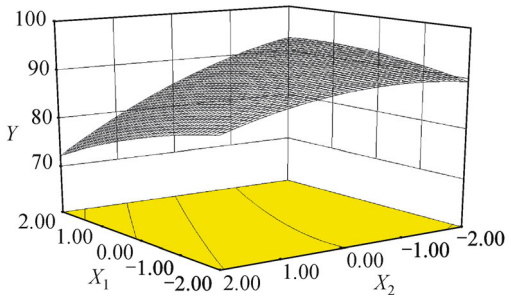

Fig. 7 The 3D response surface diagram of MO discoloration as the interaction of solution pH (X_1) and H_2O_2 concentration (X_2).

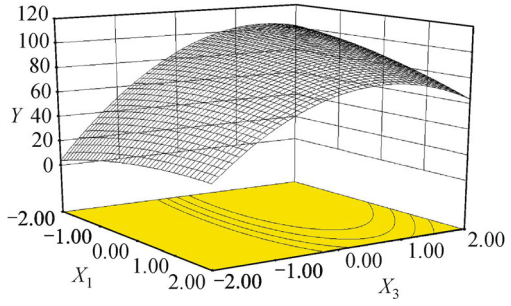

Fig. 8 The 3D response surface diagram of MO discoloration as the interaction of solution pH (X_1) and catalyst dosage (X_3).

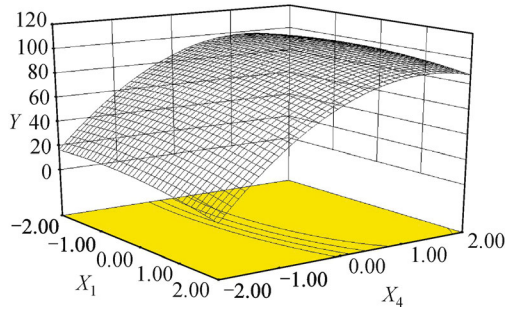

Fig. 9 The 3D response surface diagram of MO discoloration as the interaction of solution pH (X_1) and reaction time (X_4).

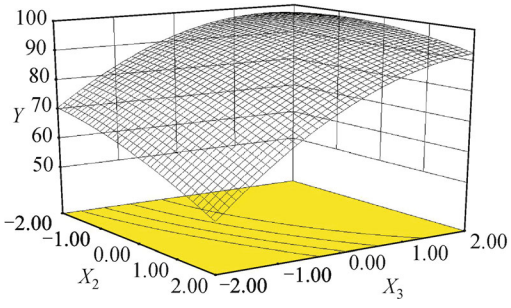

Fig. 10 The 3D response surface diagram of MO discoloration as the interaction of H_2O_2 concentration (X_2) and catalyst dosage (X_3).

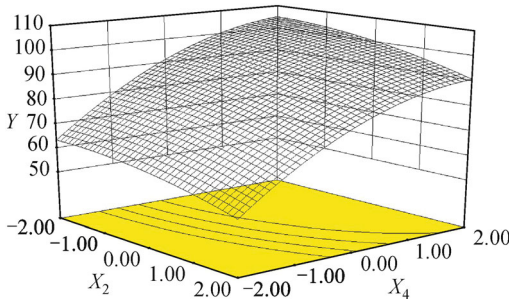

Fig. 11 The 3D response surface diagram of MO discoloration as the interaction of H_2O_2 concentration (X_2) and reaction time (X_4).

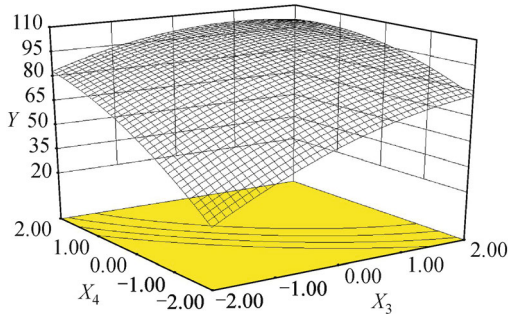

Fig. 12 The 3D response surface diagram of MO discoloration as the interaction of catalyst dosage (X_3) and reaction time (X_4).

unobvious [28]. These space diagrams reveal that MO discoloration ratio increases with the catalyst dosage and reaction time increasing, and with the solution pH decreasing. However, with the increase in H_2O_2 concentration, MO discoloration ratio first increases and then descends. The increase of H_2O_2 concentration results in an increase in the reaction activity, as expected, due to the increase of ·OH [38]. But, this does not mean that the more initial H_2O_2 concentration is, the higher the capacity for MO discoloration is. With the continuous increase in H_2O_2 concentration, active ·OH radicals would be consumed by excess H_2O_2 according to the Haber–Weiss cycle [39]. Hence, the discoloration ratio of MO would decrease with excessive increase of H_2O_2. The activity of this heterogeneous Fenton system for MO discoloration increases with the increase of catalyst dosage. The behaviour can be attributed to the fact that the more the catalyst dosage, the more active Fe sites on the catalyst surface for accelerating the decomposition of H_2O_2 (heterogeneous catalysis), and the more Fe ion leaching in the solution, leading to an increase in the number of ·OH radicals (homogeneous catalysis) [31]. Meanwhile, MO discoloration shows a strong dependence upon the solution pH and increases as

the solution pH decreases. The reaction activity of this heterogeneous Fenton-like system seems to be highest at around pH 3, consistent with the report by Hu et al. [31].

The main goal of the optimization in this study is to determine the optimum values of variables for the discoloration of MO by heterogeneous Fenton-like reaction using Fe_3O_4/MWCNTs nanocomposites as the catalyst. Based on the model prediction, the optimum conditions for the discoloration of MO in this system were determined to be of 12.3 mmol/L H_2O_2 concentration, 2.9 g/L catalyst dosage, solution pH 2.7 and 39.3 min reaction time, with the maximum predicted value for MO discoloration ratio of 101.85%. The corresponding experimental value of MO discoloration ratio under the optimum conditions was determined as 99.86%, which is very close to the predicted one with the absolute deviation of 1.99%. It confirms that RSM is a powerful and satisfactory strategy to optimize the operational parameters of MO discoloration by heterogeneous Fenton-like reaction catalyzed by Fe_3O_4/MWCNTs nanocomposites.

4 Conclusions

The preparation and characterization of Fe_3O_4/MWCNTs nanocomposites were implemented in this study, and the obtained sample was developed as a heterogeneous Fenton-like catalyst. An azo dye, MO, could be efficiently discolored by heterogeneous Fenton-like reaction catalysed by Fe_3O_4/MWCNTs nanocomposites, and 30 experiments, with 4 factors and 5 levels for each factor, were designed using CCD under the RSM. A second order polynomial model was fitted to the experimental results for the discoloration ratio of MO to obtain the predicted ones. From ANOVA, it could be known that the derived quadratic polynomial model was significant. The predicted values matched the experimental ones reasonably well with $R^2 = 0.9942$. Through constructing the plot of studentized residuals *vs.* the normal probability, a check was made for the normality assumption, which was found to be satisfied for MO discoloration as the residuals plots approximated a straight line. The 3D response surface diagrams for the interaction between two variables revealed that MO discoloration ratio increased with the catalyst dosage and reaction time increasing, and with the solution pH decreasing. However, with the increase in H_2O_2 concentration, MO discoloration ratio first increased and then descended. Based on the model prediction, the optimum conditions for the discoloration of MO by this process were determined to be of 12.3 mmol/L H_2O_2 concentration, 2.9 g/L catalyst dosage, solution pH 2.7 and 39.3 min reaction time, with the maximum predicted value for MO discoloration ratio of 101.85%. The corresponding experimental value of MO discoloration ratio under the optimum conditions was determined as 99.86%, which was very close to the predicted one with the absolute deviation of 1.99%.

Abbreviations

3D	three-dimensional
ANOVA	analysis of variance
AOP	advanced oxidation process
ATZ	atrazine
BPA	bisphenol A
CCD	central composite design
CNT	carbon nanotube
EDC	endocrine disrupting compound
FTIR	Fourier transform infrared spectroscopy
MO	methyl orange
MT	17α-methyltestosterone
MWCNT	multi-walled carbon nanotube
RSM	response surface methodology
SWCNT	single-walled carbon nanotube
TBBPA	tetrabromobisphenol A
TEM	transmission electron microscopy
UV	ultraviolet
XRD	X-ray diffraction

Acknowledgements This work was kindly supported by the National Natural Science Foundation of China (Grant Nos. 51404083 and 21273060), the Natural Science Foundation of Heilongjiang Province (E2015065) and the Program for New Century Excellent Talents in Heilongjiang Provincial Universities (1253-NCET-010).

References

[1] Konstantinou I K, Albanis T A. TiO_2-assisted photocatalytic degradation of azo dyes in aqueous solution: kinetic and mechanistic investigations – A review. Applied Catalysis B: Environmental, 2004, 49(1): 1–14

[2] Das L, Chatterjee S, Naik D B, et al. Role of surfactant derived intermediates in the efficacy and mechanism for radiation chemical degradation of a hydrophobic azo dye, 1-phenylazo-2-naphthol. Journal of Hazardous Materials, 2015, 298: 19–27

[3] Das D, Dutta R K. A novel method of synthesis of small band gap SnS nanorods and its efficient photocatalytic dye degradation.

Journal of Colloid and Interface Science, 2015, 457: 339–344

[4] Nie Y, Zhang L, Li Y-Y, et al. Enhanced Fenton-like degradation of refractory organic compounds by surface complex formation of $LaFeO_3$ and H_2O_2. Journal of Hazardous Materials, 2015, 294: 195–200

[5] Chen H, Zhang Z L, Yang Z L, et al. Heterogeneous Fenton-like catalytic degradation of 2,4-dichlorophenoxyacetic acid in water with FeS. Chemical Engineering Journal, 2015, 273: 481–489

[6] Xue X, Hanna K, Deng N. Fenton-like oxidation of rhodamine B in the presence of two types of iron (II, III) oxide. Journal of Hazardous Materials, 2009, 166(1): 407–414

[7] Rusevova K, Kopinke F D, Georgi A. Nano-sized magnetic iron oxides as catalysts for heterogeneous Fenton-like reactions – Influence of Fe(II)/Fe(III) ratio on catalytic performance. Journal of Hazardous Materials, 2012, 241-242: 433–440

[8] Xu L J, Wang J L. Fenton-like degradation of 2,4-dichlorophenol using Fe_3O_4 magnetic nanoparticles. Applied Catalysis B: Environmental, 2012, 123-124: 117–126

[9] Gao L, Zhuang J, Nie L, et al. Intrinsic peroxidase-like activity of ferromagnetic nanoparticles. Nature Nanotechnology, 2007, 2(9): 577–583

[10] Wan D, Li W B, Wang G H, et al. Adsorption and heterogeneous degradation of rhodamine B on the surface of magnetic bentonite material. Applied Surface Science, 2015, 349: 988–996

[11] Hammouda S B, Adhoum N, Monser L. Synthesis of magnetic alginate beads based on Fe_3O_4 nanoparticles for the removal of 3-methylindole from aqueous solution using Fenton process. Journal of Hazardous Materials, 2015, 294: 128–136

[12] Seyed Dorraji M S, Mirmohseni A, Carraro M, et al. Fenton-like catalytic activity of wet-spun chitosan hollow fibers loaded with Fe_3O_4 nanoparticles: Batch and continuous flow investigations. Journal of Molecular Catalysis A: Chemical, 2015, 398: 353–357

[13] Cleveland V, Bingham J P, Kan E. Heterogeneous Fenton degradation of bisphenol A by carbon nanotube-supported Fe_3O_4. Separation and Purification Technology, 2014, 133: 388–395

[14] Deng J H, Wen X H, Wang Q N. Solvothermal *in situ* synthesis of Fe_3O_4-multiwalled carbon nanotubes with enhanced heterogeneous Fenton-like activity. Materials Research Bulletin, 2012, 47 (11): 3369–3376

[15] Hu X B, Deng Y H, Gao Z Q, et al. Transformation and reduction of androgenic activity of 17α-methyltestosterone in Fe_3O_4/MWCNTs–H_2O_2 system. Applied Catalysis B: Environmental, 2012, 127: 167–174

[16] Zhou L C, Zhang H, Ji L Q, et al. Fe_3O_4/MWCNT as a heterogeneous Fenton catalyst: degradation pathways of tetrabromobisphenol A. RSC Advances, 2014, 4(47): 24900–24908

[17] Yu L, Yang X F, Ye Y S, et al. Efficient removal of atrazine in water with a Fe_3O_4/MWCNTs nanocomposite as a heterogeneous Fenton-like catalyst. RSC Advances, 2015, 5(57): 46059–46066

[18] Tristão J C, de Mendonça F G, Lago R M, et al. Controlled formation of reactive Fe particles dispersed in a carbon matrix active for the oxidation of aqueous contaminants with H_2O_2. Environmental Science and Pollution Research International, 2015, 22(2): 856–863

[19] Zhang J K, Wang G J, Zhang L P, et al. Catalytic oxidative desulfurization of benzothiophene with hydrogen peroxide catalyzed by Fenton-like catalysts. Reaction Kinetics, Mechanisms and Catalysis, 2014, 113(2): 347–360

[20] Hua Z, Ma W, Bai X, et al. Heterogeneous Fenton degradation of bisphenol A catalyzed by efficient adsorptive Fe_3O_4/GO nanocomposites. Environmental Science and Pollution Research International, 2014, 21(12): 7737–7745

[21] Zubir N A, Yacou C, Motuzas J, et al. The sacrificial role of graphene oxide in stabilising a Fenton-like catalyst GO–Fe_3O_4. Chemical Communications, 2015, 51(45): 9291–9293

[22] Zubir N A, Zhang X W, Yacou C, et al. Fenton-like degradation of acid Orange 7 using graphene oxide–iron oxide nanocomposite. Science of Advanced Materials, 2014, 6(7): 1382–1388

[23] Buang N A, Fadil F, Majid Z A, et al. Characteristic of mild acid functionalized multiwalled carbon nanotubes towards high dispersion with low structural defects. Digest Journal of Nanomaterials and Biostructures, 2012, 7: 33–39

[24] Aboutalebi S H, Chidembo A T, Salari M, et al. Comparison of GO, GO/MWCNTs composite and MWCNTs as potential electrode materials for supercapacitors. Energy & Environmental Science, 2011, 4(5): 1855–1865

[25] Gulkaya I, Surucu G A, Dilek F B. Importance of H_2O_2/Fe^{2+} ratio in Fenton's treatment of a carpet dyeing wastewater. Journal of Hazardous Materials, 2006, 136(3): 763–769

[26] GilPavas E, Dobrosz-Gómez I, Gómez-García M Á. Decolorization and mineralization of Diarylide Yellow 12 (PY12) by photo-Fenton process: the Response Surface Methodology as the optimization tool. Water Science and Technology, 2012, 65(10): 1795–1800

[27] Khataee A R, Safarpour M, Zarei M, et al. Combined heterogeneous and homogeneous photodegradation of a dye using immobilized TiO_2 nanophotocatalyst and modified graphite electrode with carbon nanotubes. Journal of Molecular Catalysis A: Chemical, 2012, 363–364: 58–68

[28] Ghanbarzadeh Lak M, Sabour M R, Amiri A, et al. Application of quadratic regression model for Fenton treatment of municipal landfill leachate. Waste Management, 2012, 32(10): 1895–1902

[29] Cao M S, Yang J, Song W L, et al. Ferroferric oxide/multiwalled carbon nanotube *vs* polyaniline/ferroferric oxide/multiwalled carbon nanotube multiheterostructures for highly effective micro-

wave absorption. ACS Applied Materials & Interfaces, 2012, 4 (12): 6949–6956

[30] Chen Y X, Gu H C. Microwave assisted fast fabrication of Fe_3O_4–MWCNTs nanocomposites and their application as MRI contrast agents. Materials Letters, 2012, 67(1): 49–51

[31] Hu X B, Liu B Z, Deng Y H, et al. Adsorption and heterogeneous Fenton degradation of 17α-methyltestosterone on nano Fe_3O_4/MWCNTs in aqueous solution. Applied Catalysis B: Environmental, 2011, 107(3–4): 274–283

[32] Chen J H, Lu D Q, Chen B, et al. Removal of U(VI) from aqueous solutions by using MWCNTs and chitosan modified MWCNTs. Journal of Radioanalytical and Nuclear Chemistry, 2013, 295(3): 2233–2241

[33] Abdullahi N, Saion E, Shaari A H, et al. Optimisation of the photonic efficiency of TiO_2 decorated on MWCNTs for Methylene Blue photodegradation. PLoS ONE, 2015, 10(5): e0125511

[34] Stobinski L, Lesiak B, Kövér L, et al. Multiwall carbon nanotubes purification and oxidation by nitric acid studied by the FTIR and electron spectroscopy methods. Journal of Alloys and Compounds, 2010, 501(1): 77–84

[35] Wang J, Li Z, Li S, et al. Adsorption of Cu(II) on oxidized multi-walled carbon nanotubes in the presence of hydroxylated and carboxylated fullerenes. PLoS ONE, 2013, 8(8): e72475

[36] Xiao D L, Dramou P, He H, et al. Magnetic carbon nanotubes: synthesis by a simple solvothermal process and application in magnetic targeted drug delivery system. Journal of Nanoparticle Research, 2012, 14(7): 984–995

[37] Azami M, Bahram M, Nouri S, et al. A central composite design for the optimization of the removal of the azo dye, methyl orange, from waste water using the Fenton reaction. Journal of the Serbian Chemical Society, 2012, 77(2): 235–246

[38] Idel-aouad R, Valiente M, Yaacoubi A, et al. Rapid decolourization and mineralization of the azo dye C.I. Acid Red 14 by heterogeneous Fenton reaction. Journal of Hazardous Materials, 2011, 186(1): 745–750

[39] Xu H Y, Shi T N, Wu L C, et al. Discoloration of methyl orange in the presence of schorl and H_2O_2: Kinetics and mechanism. Water, Air, and Soil Pollution, 2013, 224(10): 1740